Research Square

Preprints are preliminary reports that have not undergone peer review.
They should not be considered conclusive, used to inform clinical practice,
or referenced by the media as validated information.

# Roll-to-Plate Fabrication of Gold Nanopillar SERS Chips for Phthalate Detection and Classification

**Yeonghee Jeong**
Konkuk University
**Hye-Seong Cho**
Konkuk University
**Jong Hun lm**
Company of Global Zeus
**Jaehi Kim**
Konkuk University
**Sung-Kyu Lee**
Konkuk University
**Cho-Hee Yang**
Konkuk University
**Sungwoo Park**
Konkuk University
**Geunhyeong An**
Kangwon National University
**Hyejin Chang**
Kangwon National University
**Heung Su Jung**
Company of Global Zeus
**Bong-Hyun Jun**
b.jun@konkuk.ac.kr

Konkuk University

**Research Article**

**Keywords:**

**Posted Date:** November 13th, 2026

**DOI:** https://doi.org/10.21203/rs.3.rs-11571597/v1

**License:** This work is licensed under a Creative Commons Attribution 4.0 International License.
Read Full License

**Additional Declarations:** No competing interests reported.

# Abstract

Surface-enhanced Raman scattering (SERS) is a detection technique that enables rapid and non-destructive analysis of samples. To overcome the high cost and long fabrication time associated with conventional SERS substrate fabrication processes and to facilitate commercialization, extensive research has been conducted on the development of SERS substrates suitable for large-scale production. Although significant progress has been made in the mass production of SERS substrates using various fabrication methods, including lithography and nanoimprinting, high fabrication costs and long processing times are still required during pattern formation and subsequent metal deposition, remaining major challenges for commercialization. In this study, to address these limitations, a 6-inch scale Au Nanopillar SERS substrate (Au NSS) was fabricated by patterning nanopillar structures over a large area using a roll-to-plate process, followed by Au sputtering, thereby simplifying the fabrication process and enabling rapid and cost-effective production. The fabricated nanopillar structures induced localized electromagnetic field enhancement and exhibited SERS activity. The resulting Au Nanopillar SERS chip (Au NSC) achieved a limit of detection $1.53 \times 10^{-6}$ M for rhodamine 6G. In addition, the detection performance of the Au NSC was evaluated for four phthalates widely used in industrial applications confirming the feasibility of detecting each compound. Furthermore, AI-based analysis was applied to classify the four phthalates at a concentration of 50 ppm. These results demonstrate the potential of the developed Au NSC as a low-cost, large-area, and mass-producible SERS analytical platform for practical applications in industrial environments.


# Introduction

Surface-enhanced Raman scattering (SERS) is a non-destructive and rapid analytical technique with high potential for applications in various fields, including food safety, quality control, medical diagnostics, forensics, and environmental monitoring[1–5]. However, despite their high detection sensitivity, conventional SERS substrates often face challenges in achieving signal uniformity and reproducibility. Furthermore, their fabrication typically involves time-consuming and costly processes, along with limitations in the achievable substrate area, thereby hindering their commercialization. Accordingly, various fabrication technologies capable of producing large-area SERS substrates have been actively investigated to facilitate the commercialization of SERS-based platforms[6–8]. Although large-area SERS substrates can be fabricated using various top-down techniques, including lithography- and etching-based processes, conventional high-resolution fabrication approaches often require sophisticated equipment and complex processing steps, resulting in increased fabrication time and cost and thereby posing challenges to scalable manufacturing[9–13].

To address these limitations, nanoimprint technology has been actively investigated for SERS chip fabrication because it enables repeated replication of micro- and nanostructures over large areas[14–17].

Among various nanoimprint techniques, roller-based nanoimprint processes have attracted considerable attention because of their high productivity and repeatable replication capability, and they can typically

be classified into roll-to-roll (R2R) and roll-to-plate (R2P) processes[18,19]. The R2R process offers high productivity through continuous processing of flexible films; however, it requires precise control of web tension and transport speed and is less suited to direct patterning on discrete flat substrates[5,20,21]. In contrast, the R2P process enables micro- and nanostructures to be transferred onto discrete flat substrates using a roller-based imprinting configuration, while retaining the high-throughput characteristics of nanoimprint processing. In addition, nanoimprint processes are compatible with a broad range of substrate and functional materials and can be integrated with subsequent fabrication steps such as etching and metal deposition[14,18,22]. Recently, Zhang et al. fabricated a SERS chip by producing a microarray structure using an R2P process followed by the growth of Ag nanoparticles[15]. However, this approach required an additional Ag nanoparticle growth step, increasing the overall fabrication complexity.

In this study, to address these limitations, a 6-inch scale Au Nanopillar SERS substrate (Au NSS) was fabricated by patterning nanopillar structures on a wafer surface using an R2P process, followed only by simple sequential Ti and Au sputtering process. The fabricated nanopillar structures can induce localized electromagnetic field enhancement, enabling sufficient SERS activity to be achieved through Metal sputtering without requiring an additional metal nanoparticle growth process. In addition, the SERS detection performance was evaluated for four phthalates widely used in industrial applications dibutyl phthalate (DBP), benzyl butyl phthalate (BBP), diisobutyl phthalate (DIBP), and di(2-ethylhexyl) phthalate (DEHP), and detection was successfully achieved at concentrations below the relevant regulatory limits. Furthermore, by combining SERS spectra with AI-based analysis, the four phthalates could be classified (Fig. 1). These results demonstrate the potential for scalable fabrication and industrial applications.

# Methods

## - Materials

100 × 100 mm single-pass anodic aluminum oxide (AAO), UV-curable resin (Mins-311), LS40 surface release agent, Benzyl butyl phthalate (BBP), dibutyl phthalate (DBP), di(2-ethylhexyl) phthalate (DEHP), diisobutyl phthalate (DIBP), ethanol (EtOH, ≥ 99.9%) were purchased from Sigma-Aldrich (St. Louis, MO, USA). Rhodamine 6G (R6G) was purchased from TCI (Tokyo, Japan).

## - Instrument

Nanoimprint lithography (NIL) was performed using a GIGALANE Nano imprinter. Metallic layer was deposited by sputtering. The morphology and elemental distribution of the Au NSC were characterized using field-emission scanning electron microscopy (FE-SEM, SIGMA, UK) and focused ion beam energy-dispersive X-ray spectroscopy (FIB–EDS, AURIGA, Germany), respectively, Optical reflectance spectra was recorded using a UV–Vis–NIR spectrophotometer (PerkinElmer, USA). Raman spectra were acquired using a portable Raman spectrometer (i-Raman Prime, B&W Tek Inc., Newark, DE, USA). All data

processing and deep neural network (DNN) modeling were performed using Python 3.11.15 with TensorFlow/Keras 2.21.0, scikit-learn 1.8.0, NumPy 2.4.6, and pandas 3.0.3.

## - Fabrication of the Au NSS

The Au NSS was fabricated using nanoimprint lithography (NIL) with a 100 × 100 mm single-pass anodic aluminum oxide (AAO) template, a UV-curable resin (Mins-311), and LS40 surface release agent. The LS40 release agent was applied to facilitate demolding and improve pattern transfer. Nanoimprinting was performed using a GIGALANE NIL system, followed by UV curing and demolding to obtain the replicated nanostructures. Subsequently, a 20 nm Ti layer was deposited by sputtering, followed by a 150 nm Au layer to form the plasmonically active surface.

## - Sample preparation and SERS measurements

R6G and phthalates were dissolved in ethanol to prepare solutions at the desired concentrations. For Raman analysis, 10 μL of each analyte solution was drop-cast onto an Au NSC and allowed to spread evenly across the chip surface. The deposited samples were completely dried at room temperature for approximately 10 min. Subsequently, 20 μL of 10mM phosphate-buffer or 0.5% Ethylene Glycol was added to the Au NSC, and Raman measurements were performed while the chip surface remained covered with buffer solution.

Raman spectra were acquired using a Raman spectrometer (i-Raman Prime 785, B&W TEK, Newark, DE, USA) equipped with a 785 nm excitation laser. R6G solutions were prepared at concentrations ranging from $10^{-3}$ to $10^{-7}$ M, whereas each phthalates solution was prepared at concentrations ranging from $10^{-3}$ to $10^{-6}$ M. For limit of detection (LOD) evaluation, Raman spectra were collected at three randomly selected positions for each analyte concentration. The calibration curve for each analytical method was determined by sigmoidal curve fitting **(**Fig. 3A, C**)**. The calibration curve equation is expressed as follows:

$$Raman\ intensity = A2 + \frac{(A1 - A2)}{(1 + (X/X_0)^P} \qquad (1)$$

The LOD of each system was calculated based on calibration curves **(Supporting Table S1)**. The intra-chip uniformity of the SERS response was evaluated using R6G by collecting spectra from 50 randomly selected positions across a single Au NSC. Chip-to-chip reproducibility was evaluated using 10 Au NSCs, with spectra collected from five randomly selected positions on each chip. The relative standard deviation (RSD) of the R6G Raman signal intensities was calculated using Eq. (2):

$$RSD = \frac{\sigma}{\mu} \times 100\% \qquad (2)$$

where σ and μ represent the standard deviation and mean intensity of the R6G Raman peak at 1508 $cm^{-1}$, respectively.

## - Characterization of Au NSC

The morphology, structural dimensions, elemental distribution, and optical properties of the Au NSC were systematically characterized. Surface and cross-sectional images were acquired using field-emission scanning electron microscopy (FE-SEM, SIGMA, UK), and the height, width, and inter-pillar gap of the Au nanopillars were determined from the resulting images using ImageJ software. For each structural parameter, 100 individual measurements were analyzed, and the results are expressed as the mean ± standard deviation. Elemental mapping was performed using a focused ion beam energy-dispersive X-ray spectroscopy (FIB–EDS, AURIGA, Germany), while the optical reflectance spectra of the Au NSC were recorded using a UV–Vis–NIR spectrophotometer (PerkinElmer, USA).

# - DNN modeling and validation

The DNN model for the classification of phthalates was developed using in-house Python code. A total of 250 SERS spectra were acquired using a Raman spectrometer, comprising 50 spectra for each of the four phthalates (DBP, BBP, DIBP, and DEHP) at 50 ppm and 50 spectra from the Au substrate. Each spectrum consisted of 723 spectral features within the Raman shift range of 400–1800 $cm^{-1}$. The DNN consisted of two hidden layers containing 32 and 16 neurons, respectively, with rectified linear unit (ReLU) activation functions. A dropout layer with a dropout rate of 0.3 was applied after the first hidden layer to reduce overfitting. The output layer consisted of five neurons with a softmax activation function for five-class classification. The model was optimized using the Adam optimizer with a learning rate of 0.001, and categorical cross-entropy was used as the loss function.

For model training and evaluation, the dataset was divided into training and test sets at a ratio of 80:20 using stratified random sampling to preserve the class distribution. Spectral features were standardized using the mean and standard deviation derived from the training set, and the same transformation was subsequently applied to the test set. Within the training set, 20% of the data were used as a validation set during model training. Early stopping was applied by monitoring the validation loss, and training was terminated when the validation loss did not improve for 20 consecutive epochs. The model weights corresponding to the lowest validation loss were restored. The model was trained for a maximum of 300 epochs with a batch size of 16.

To assess the stability of classification performance across repeated modeling procedures, the entire train–test splitting, preprocessing, model training, and evaluation procedure was repeated 100 times. For each iteration, the random seed was set to the corresponding iteration number to enable reproducible data partitioning and model training.

For each iteration, classification performance was evaluated using accuracy, receiver operating characteristic (ROC) analysis, and a confusion matrix based on the corresponding test set. Class-specific ROC curves and area under curve (AUC) values were calculated using a one-vs-rest approach. To generate representative ROC curves across the 100 iterations, the true positive rates (TPRs) of individual ROC curves were interpolated onto a common false positive rate (FPR) grid and averaged at each FPR point. AUC values were summarized as the mean ± standard deviation. Non-normalized confusion matrices containing the numbers of predicted samples for each class were calculated for individual iterations and subsequently averaged element-wise across the 100 iterations.

## Results and discussion

# Fabrication and characterization of Au NSC

6-inch-scale Au NSS was fabricated using a R2P nanoimprint process. First, a polymer resist was coated onto the wafer surface, followed by rolling a roller mold containing nanopatterns over the resist-coated wafer to transfer the nanopillar patterns onto the wafer surface. Subsequently, the patterned wafer was exposed to UV light to induce photopolymerization, thereby fixing and stabilizing the nanopillar structures. To improve adhesion between the patterned nanopillar structures and Au, a Ti layer was first deposited, followed by Au sputtering to form an Au shell, completing the fabrication of the Au NSS (Fig. 2A).

Figure 2B**(a)** shows the 6-inch scale Au NSS fabricated by Au sputtering. The fabricated wafer was cut into 5 × 5 mm² pieces to obtain Au NSC with uniform dimensions, allowing approximately 400 chips to be produced from a single 6-inch scale (Fig. 2B **(b)**).

The morphology of the nanopillar structures formed on the surface and the successful transfer of the patterns were analyzed using SEM. The top-view and side-view SEM images confirmed that the nanopillar patterns were successfully transferred onto the wafer surface through the nanoimprint process (Fig. 2C **(a, b)**).

In addition, the dimensions of the transferred nanopillar structures were quantitatively analyzed from the SEM images using ImageJ. The diameter and height of the nanopillars, as well as the gap distance between adjacent nanopillars, were measured. Each structural parameter was analyzed using a total of 100 nanopillars. The average diameter of the nanopillars was measured to be 120.2 nm with a standard deviation of 10.3 nm, while the average height was 177.6 nm with a standard deviation of 17.1 nm (Fig. 2D **(a, b)**). The gap distance between the nanopillars was measured to be 8.4 ± 3.4 nm, which was comparable to that of the nanopillar pattern formed on the roller mold. These results confirmed that the nanopillar pattern of the roller mold was successfully transferred onto the wafer surface with high reproducibility (Fig. 2D **(c)**).

EDS analysis was performed to confirm whether Au and Ti were deposited onto the surface of the polymer nanopillar structures by sputtering. The EDS analysis showed clear Au and Ti signals originating

from the sputtered Au and Ti layers, respectively, along with C and O signals derived from the polymer substrate. Weight percentage analysis showed that Au accounted for 93.79 wt%, while C, O, and Ti accounted for 4.57 wt%, 0.77 wt%, and 0.86 wt%, respectively. These results demonstrated that Ti and Au deposited by sputtering were successfully incorporated into the polymer nanopillar structures **(Supporting figure S1)**.

Finally, to investigate whether the nanopillar pattern of the Au NSC formed an optical structure capable of contributing to electromagnetic field enhancement, the reflectance spectrum of the Au NSC was compared with that of a planar Au chip fabricated by Au sputtering without nanopillar structures[23–25]. The planar Au chip and Au NSC exhibited minimum reflectance values of 31.61% and 12.7%, respectively, at wavelengths around 500 nm. The planar Au chip exhibited a sharp increase in reflectance at approximately 500 nm beyond the absorption region associated with the intrinsic interband transitions of Au. In contrast, the Au NSC exhibited substantially lower reflectance than the planar Au chip over the entire measured wavelength range due to the formation of the nanopillar structure. These results demonstrate that the Au NSC nanopillar structure exhibits optical characteristics favorable for light trapping and LSPR excitation. **(**Fig. 2E**)**.

# SERS perfomance and phthalate detection of Au NSC

To evaluate the SERS performance of the Au NSC, concentration-dependent SERS measurements were performed using R6G as a standard analyte. For quantitative analysis, the intensity of the characteristic Raman peak of R6G at 1508 $cm^{-1}$ was used to determine the limit of detection[26]. The relationship between the peak intensity and R6G concentration showed $R^2$ value of 0.99, and the limit of detection (LOD) was determined to be $1.53 \times 10^{-6}$ M **(**Fig. 3A**)**.

Signal reproducibility is another important factor in evaluating SERS performance because SERS signals are highly sensitive to variations in nanostructure size and understructure gap distance. For large-area SERS chip fabrication, uniform formation of nanostructures over the entire substrate is essential, as structural uniformity is directly related to SERS signal reproducibility. To evaluate the signal reproducibility of the Au NSC within a single chip, SERS measurements were randomly performed at 50 locations **(Supporting figure S2)**. The resulting RSD was 9.13%, which was lower than 10%, confirming high SERS signal reproducibility within a single Au NSC. In addition, to evaluate the reproducibility of the 6-inch scale Au NSS, 10 Au NSCs were randomly selected and analyzed **(Supporting figure S3)**. The calculated RSD was 9.21%, demonstrating high SERS signal reproducibility across the Au NSS **(**Fig. 3B**)**.

To evaluate the applicability of the Au NSC for the detection of hazardous substances, the LOD for four phthalates widely used as plasticizers, namely DBP, BBP, DIBP, and DEHP, were analyzed. The characteristic Raman peak at 1040 $cm^{-1}$ was used for quantitative analysis of the four phthalates. All four phthalates showed a high relationship between concentration and SERS signal, with $R^2$ values of 0.99. The calculated LODs were $3.69 \times 10^{-5}$ for DBP **(**Fig. 3C**)**, $2.36 \times 10^{-5}$ for BBP **(**Fig. 3D**)**, $7.17 \times 10^{-5}$ for DIBP **(**Fig. 3E**)**, and $2.67 \times 10^{-5}$ for DEHP **(**Fig. 3F**)**[27–29]. These results demonstrate the potential of

the Au NSC for phthalate detection. Further studies using extracts from real products are required to evaluate its applicability to regulatory screening.

These results demonstrate that the fabricated Au NSC can be utilized as a SERS platform for phthalate screening.

# Classification of phthalates by using DNN

As a practical application of the fabricated Au NSC, label-free SERS-based classification of phthalates was conducted using a DNN model. Four phthalates, DBP, BBP, DIBP, and DEHP were selected as the target analytes. Raman spectra were acquired after applying each phthalate to the fabricated Au NSC, along with spectra of the bare Au NSC. The representative Raman shifts were identified by comparing each class-averaged Raman spectrum with the overall mean spectrum, and the resulting class-associated spectral differences were summarized **(Supporting Table S2)**. For DNN-based classification, the acquired full spectra were used as input data to classify the five sample classes **(**Fig. 4A**)**. The entire modeling procedure, including train–test splitting, model training, and performance evaluation, was repeated 100 times, and the resulting classification performance was summarized across the iterations **(**Fig. 4B–D**)**.

Figure 4B shows the mean ROC curves obtained from the 100 iterations, together with the mean AUC value for each class. The mean AUC values for DBP, BBP, DIBP, DEHP, and the substrate were 0.967, 0.998, 0.979, 1.000, and 0.992, respectively, with all classes exhibiting mean AUC values above 0.95. These results indicate that the DNN model achieved high one-vs-rest discriminative performance across all five classes. The mean confusion matrix further revealed class-dependent differences in classification performance **(**Fig. 4C**)**. The classification rates for DEHP, BBP, DIBP, and DBP were 99.4%, 95.1%, 86.1%, and 72.2%, respectively, while the bare Au substrate exhibited a classification rate of 92.6%. Notably, DBP showed the lowest classification rate among the four phthalates, with 12.1% and 10.0% of its spectra misclassified as DIBP and the bare Au substrate, respectively. The relatively high confusion between DBP and DIBP may partly originate from their structural similarity, as both compounds share the same phthalate backbone and differ primarily in the configuration of their butyl side chains. However, the appreciable misclassification of DBP as the bare substrate indicates that structural similarity alone cannot fully explain its lower classification rate. Across the 100 iterations, the DNN model achieved a mean accuracy of 0.891 ± 0.045, indicating high overall classification performance across repeated modeling procedures **(**Fig. 4D**)**. Overall, the DNN model effectively identified most phthalate classes based on the SERS spectra; however, the relatively low classification accuracy for DBP indicates that there is still room for improvement in achieving consistent five-class classification. Nevertheless, these results demonstrate that the combination of the Au NSC and AI-based analysis can be effectively used to distinguish hazardous substances with similar Raman spectral features and suggest the potential of this approach for future application in real industrial environments.

# Conclusion

In this study, a low-cost, large-area, and mass-producible 6-inch-scale Au NSC was fabricated using an R2P nanoimprint process and Au sputtering. The nanopillar structures formed through roll-based patterning and Au deposition induced localized electromagnetic field enhancement and exhibited SERS activity, achieving a detection limit of $10^{-6}$ M for R6G. In addition, the SERS detection performance was evaluated for four phthalates, and AI-based analysis demonstrated the potential to distinguish phthalates with similar Raman spectral features. Therefore, the R2P-based Au NSC proposed in this study combines a simple fabrication process with large-area manufacturing and mass-production capabilities and demonstrates its potential as a practical SERS analytical platform for identifying hazardous substances with similar Raman peaks through integration with AI-based analysis.

## Declarations

# Author contributions

Author contributions All authors contributed to the study conception and design. Conceptualization: [Y. Jeong, H. Cho], Methodology: [Y. Jeong, H. Cho, J. Kim, S. Lee, C. Yang], Formal analysis and investigation: [Y. Jeong, H. Cho, S. Park, G. An], Resource: [H. Chang, J. lm, H. Jeong], Writing original draft preparation: [Y. Jeong, H. Cho, J. lm, H. Jeong], Writing - review and editing: [Y. Jeong, H. Cho, B. Jun], Supervision: [B. Jun]

# Declarations

The authors have no competing interests to declare that are relevant to the content of this article.

**Conflict of interest**

The authors declare no conflict of interests.

# Author Contribution

Author contributions All authors contributed to the study conception and design. Conceptualization: [Y. Jeong, H. Cho], Methodology: [Y. Jeong, H. Cho, J. Kim, S. Lee, C. Yang], Formal analysis and investigation: [Y. Jeong, H. Cho, S. Park, G. An], Resource: [H. Chang, J. lm, H. Jeong], Writing original draft preparation: [Y. Jeong, H. Cho, J. lm, H. Jeong], Writing - review and editing: [Y. Jeong, H. Cho, B. Jun], Supervision: [B. Jun]

# Acknowledgements

This work was supported by the National Research Foundation of Korea(NRF), funded by the Korean government (MSIT) (RS-2023-00222910 andRS-2025-00558156); the Korea Health Industry Development Institute(KHIDI), funded by the Ministry of Health and Welfare, Republic of Korea(Grant No. RS-2026-25610538); and the Konkuk University ResearcherFund in 2024 (Project No. 2024-A019-0317).

# Data Availability

The datasets generated and/or analyzed during the current study are available from the corresponding author upon reasonable request.

## References

1. Yang, C. H. *et al.* Silica/Nanographene Oxide Nanocomposites Decorated With Au@ Ag Nanoparticles as Surface-Enhanced Raman Scattering Tags for Highly Sensitive Quantitative Lateral Flow Immunoassays. *Small Structures* **7**, e70569 (2026).
2. Park, M., Kim, Y.-S., Kim, S. & Lim, J. Y. Ultra-sensitive, on-site pesticide detection for environmental and food safety monitoring using flexible cellulose nano fiber/Au nanorod@ Ag SERS sensor. *Journal of Hazardous Materials* **487**, 137197 (2025).
3. Ozorio, M. *et al.* ZnO Nanorod/Ag Nanoparticle Functionalized Paper Substrate for Sensitive SERS Detection of Environmental Contaminants. *ACS Applied Nano Materials* **8**, 10434–10447 (2025).
4. de Souza, M. A. *et al.* Photochemically-made gold nanorods for adsorption and SERS detection of cocaine and benzoylecgonine in latent fingerprints. *RSC advances* **15**, 44164–44172 (2025).
5. Barcelo, S. & Li, Z. Nanoimprint lithography for nanodevice fabrication. Nano Convergence 3, 21 (2016).
6. Das, A., Gupta, N., Agrawal, A. K. & Dhawan, A. Large-area and low-cost SERS substrates based on a gold-coated nanostructured surface fabricated on a wafer-scale. *RSC advances* **12**, 9645–9652 (2022).
7. Wu, L. *et al.* Fabrication of wafer-scale ordered micro/nanostructures for SERS substrates using rotational symmetry cantilever-based probe lithography. *Applied Surface Science* **626**, 157220 (2023).
8. Laariedh, F., Sow, I., Ferchichi, A., Zelsmann, M. & Boussey, J. Large-area, cost-effective Surface-Enhanced Raman Scattering (SERS) substrates fabrication. *Microelectronic Engineering* **145**, 124–127 (2015).
9. Soufi, G. *et al.* SERS-based nano-and microsystems toward biomedical applications. *Small* **22**, e73304 (2026).
10. Luo, S. *et al.* High-throughput fabrication of triangular nanogap arrays for surface-enhanced Raman spectroscopy. *ACS nano* **16**, 7438–7447 (2022).

11. Cialla-May, D. *et al.* Biomedical SERS–the current state and future trends. *Chemical Society Reviews* **53**, 8957–8979 (2024).
12. Langer, J. *et al.* Present and future of surface-enhanced Raman scattering. *ACS nano* **14**, 28–117 (2020).
13. Eom, S.-J., Seo, H.-S., Devaraj, V. & Lee, J.-M. Wafer-scale, simple, and low-cost fabrication of uniform SERS substrates: A review and perspective. *Current Applied Physics* (2026).
14. Suresh, V., Ding, L., Chew, A. B. & Yap, F. L. Fabrication of large-area flexible SERS substrates by nanoimprint lithography. *ACS Applied Nano Materials* **1**, 886–893 (2018).
15. Zhang, C. *et al.* Highly sensitive and reproducible SERS substrates based on ordered micropyramid array and silver nanoparticles. *ACS applied materials & interfaces* **13**, 29222–29229 (2021).
16. Daskalova, D., Özyurt, M. S., Lerch, H., Plachetka, U. & Lemme, M. C. Periodic and Statistically Distributed Surface Texturing of Surface-Enhanced Raman Spectroscopy (SERS) Sensors with Spatially Selective Signal Mapping. *Advanced Physics Research* **5**, e00124 (2026).
17. Xue, X. *et al.* High-uniformity, low-cost, ultra-dense arrays of Au-capped plastic nanopillars fabricated via nanoimprint lithography as reliable SERS substrates. *Spectrochimica Acta Part A: Molecular and Biomolecular Spectroscopy* **335**, 125989 (2025).
18. Kooy, N., Mohamed, K., Pin, L. T. & Guan, O. S. A review of roll-to-roll nanoimprint lithography. *Nanoscale research letters* **9**, 320 (2014).
19. Peng, Z. *et al.* Continuous roller nanoimprinting: next generation lithography. *Nanoscale* **15**, 11403–11421 (2023).
20. Jeon, H. *et al.* Control methodology for tensioned web considering thermal behavior in roll-to-roll manufacturing systems. *Engineering Science and Technology, an International Journal* **46**, 101508 (2023).
21. Gafurov, A. N. *et al.* AI-driven digital twin for autonomous web tension control in Roll-to-Roll manufacturing system. *Scientific reports* **15**, 24096 (2025).
22. Ding, Y.-C. & Lee, Y.-C. Nanoimprinting and backside ultraviolet lithography for fabricating metal nanostructures with higher aspect ratio. *Nanotechnology* **36**, 045302 (2025).
23. Liu, X. *et al.* Tailored Surface-Enhanced Raman Nanopillar Arrays Fabricated by Laser-Assisted Replication for Biomolecular Detection Using Organic Semiconductor Lasers. *ACS Nano* **9**, 260–270 (2014).
24. Rastogi, R. *et al.* Analyte Co-localization at Electromagnetic Gap Hot-Spots for Highly Sensitive (Bio)molecular Detection by Plasmon Enhanced Spectroscopies. *ACS Applied Materials & Interfaces* **13**, 9113–9121 (2021).
25. Dhawan, A., Gerhold, M. & Vo-Dinh, T. Theoretical simulation and focused ion beam fabrication of gold nanostructures for surface-enhanced Raman scattering (SERS). *Nanobiotechnology* **3**, 164–171 (2007).

26. Wang, J. *et al.* Uniformly aligned Ag NPs/graphene paper for enhanced SERS detection of pesticide residue. *Spectrochimica Acta Part A: Molecular and Biomolecular Spectroscopy* **329**, 125535 (2025).
27. Wang, B. *et al.* Enhancing SERS Sensitivity in N-Graphene Hydrangea by Synergistic Charge-Transfer and Excitation Light Absorption. *Small Structures* **5**, 2300418 (2024).
28. Dhillon, A. K. *et al.* Surface-Engineered Hydrophobic Porous Organic Polymer for Enhanced SERS Detection of Plasticizers. *Advanced Optical Materials* **13**, e00856 (2025).
29. Hu, X. *et al.* Bimetallic plasmonic Au@Ag nanocuboids for rapid and sensitive detection of phthalate plasticizers with label-free surface-enhanced Raman spectroscopy. *Analyst* **144**, 3861–3869 (2019).

# Figures

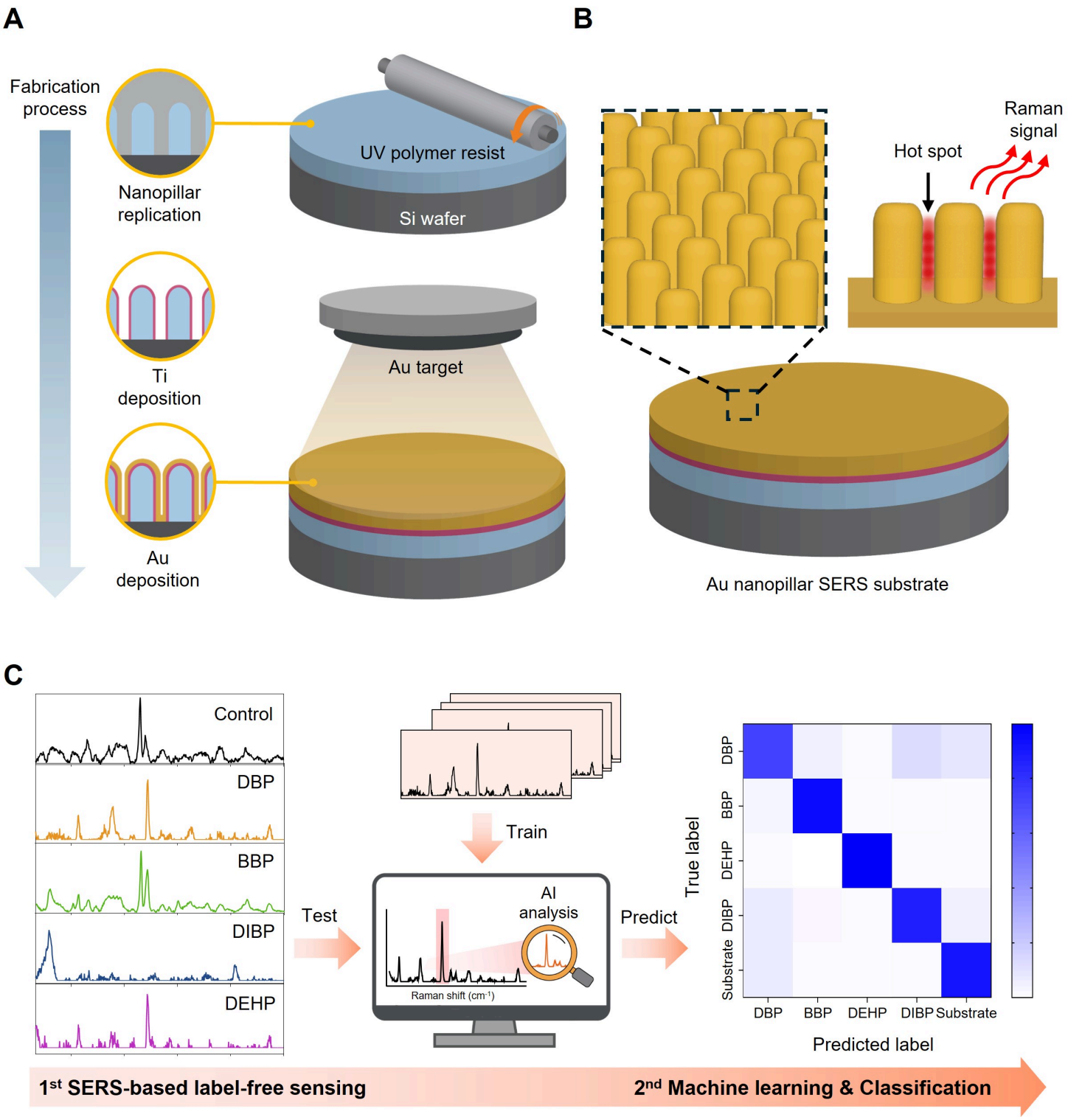
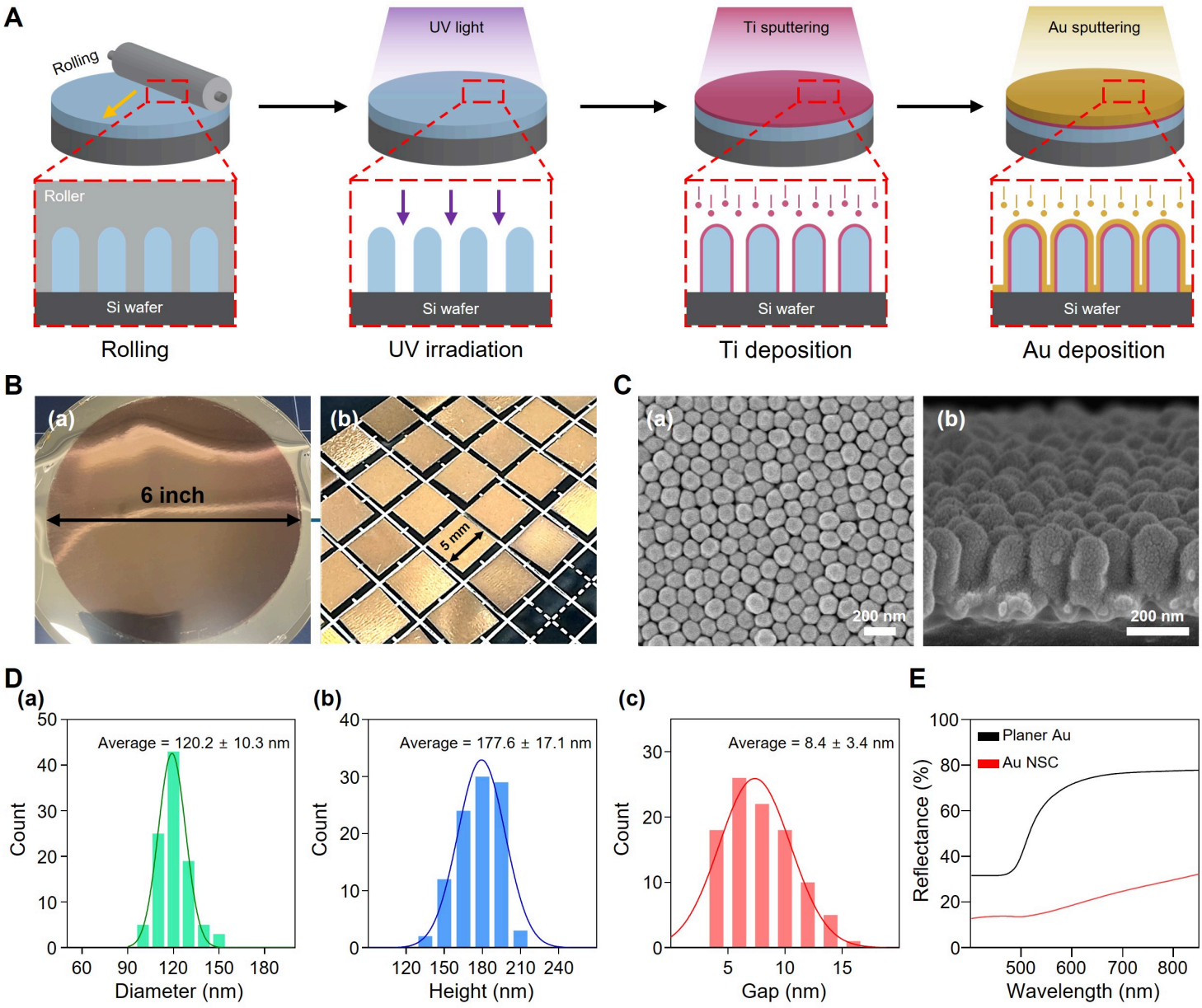


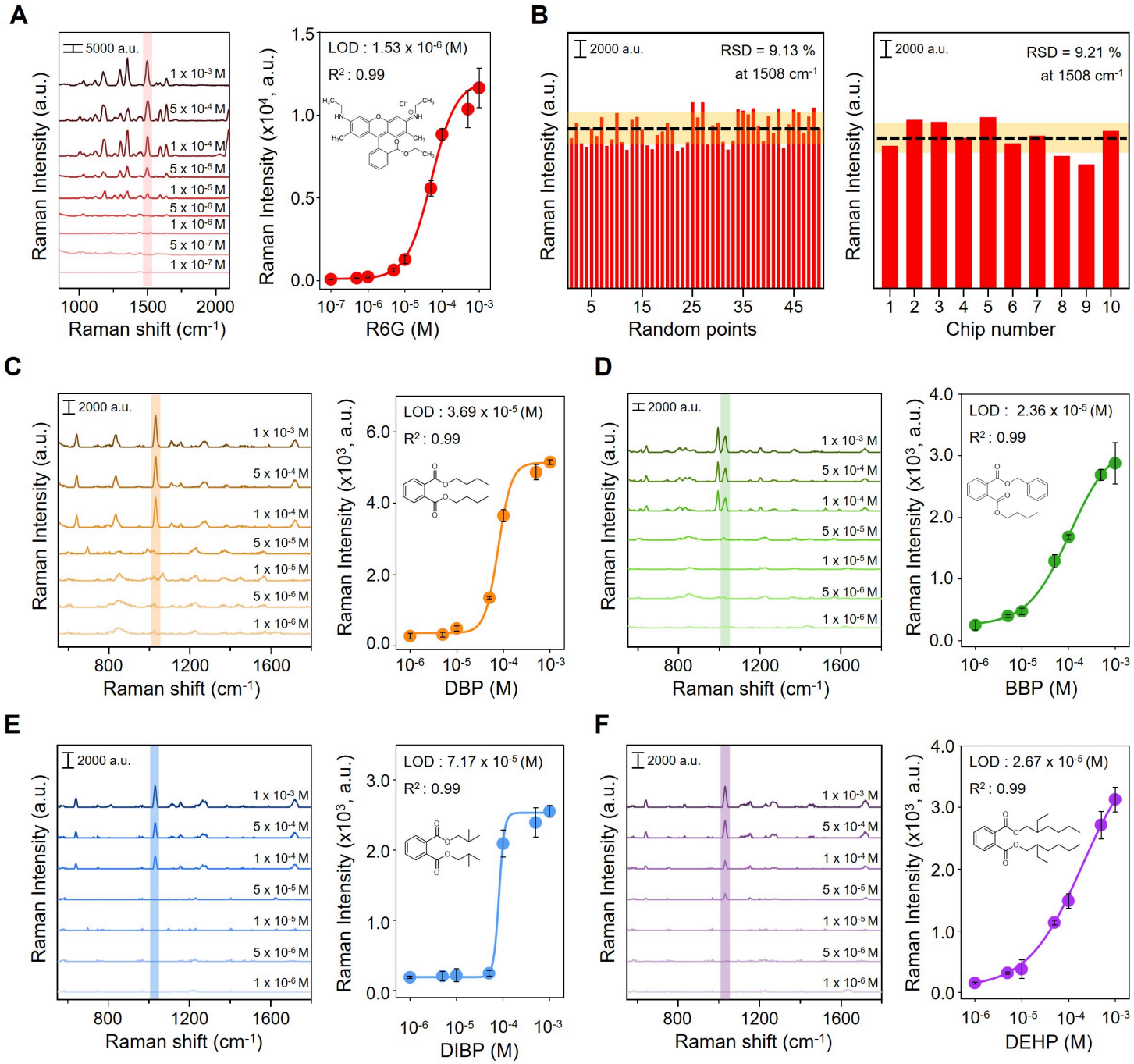

**Figure 1**

**Schematic illustration of Au nanopillar Surface-enhanced Raman scattering (SERS) substrate (Au NSS) fabrication and AI-based SERS detection of phthalates.** Fabrication process of Au NSS. **A** Label-free SERS detection of phthalates using Au nanopillar SERS chip (Au NSC). **B** AI-based classification of phthalates. **C**




## Figure 2

**Fabrication and characterization of Au NSC. A** Roll-to-plate fabrication process of Au NSC. **B** Images of Au NSS (a) and Au NSC (b). **C** SEM images of the Au nanopillar structures: (a) top view and (b) side view. **D** Quantitative structural analysis and optical characterization of the Au NSC: distributions of nanopillar diameter (a), nanopillar height (b), and inter-nanopillar gap (c). **E** Reflectance spectra of the planar Au chip and Au NSC.




## Figure 3

**SERS performance of the Au NSC for R6G and phthalate detection. A** Calibration curve and concentration-dependent SERS spectra of R6G. **B** Reproducibility of the SERS signals measured at multiple positions and across different Au NSC. **C-F** Calibration curves and concentration-dependent SERS spectra of DBP, BBP, DIBP, and DEHP.

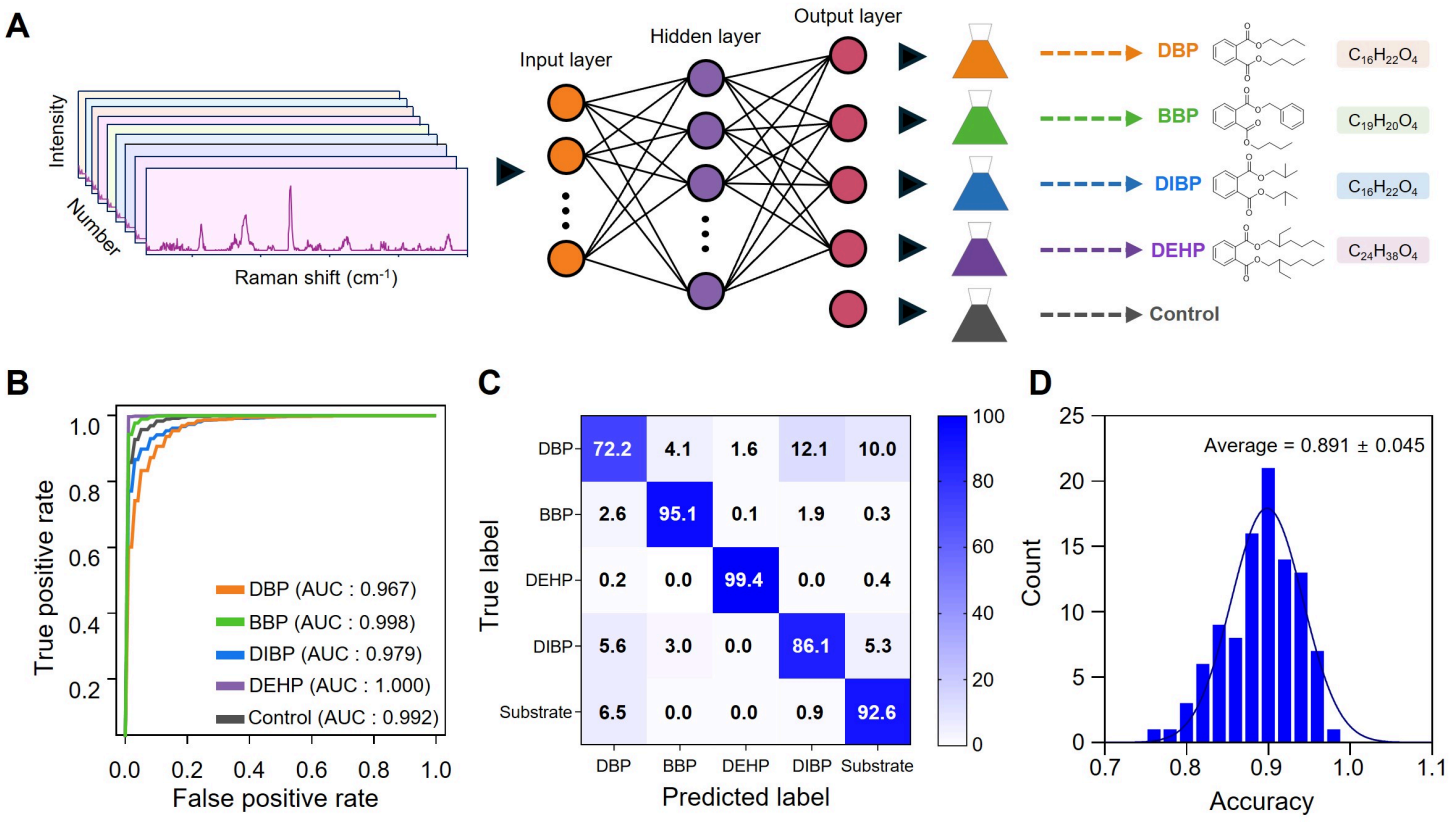



**Figure 4**

**DNN based phthalate classification. A** Schematic illustration of the workflow for DNN-based phthalate classification. **B** Mean ROC curves for the four phthalates and control samples. **C** Mean Confusion matrix illustrates the classification performance of the DNN model for the four phthalates and the control sample. **D** Histogram of classification accuracy obtained over 100 DNN modeling iterations.

# Supplementary Files

This is a list of supplementary files associated with this preprint. Click to download.

- AuSERSchipsupply.pptx